August 8, 2007

Identity Profiling of Cell Surface Markers by Multiplex Gold Nanorod Probes

Chenxu Yu, *Purdue University*
Harikrishna Nakshatri, *Indiana University*
Joseph Irudayaraj, *Purdue University*

NANO LETTERS

2007
Vol. 7, No. 8
2300−2306

Identity Profiling of Cell Surface Markers by Multiplex Gold Nanorod Probes

Chenxu Yu,[†,‡] Harikrishna Nakshatri,[§,||,⊥,#] and Joseph Irudayaraj*[,†,‡]

Department of Agricultural and Biological Engineering and Bindley Biosciences Center, Purdue University, 225 South University Drive, West Lafayette, Indiana 47906, Department of Surgery, Walther Oncology Center, Department Biochemistry and Molecular Biology, Indiana University School of Medicine, Indianapolis, Indiana 46202, Walther Cancer Institute, Indianapolis, Indiana 46208

Received April 16, 2007; Revised Manuscript Received May 18, 2007

ABSTRACT

Gold nanorod molecular probes (GNrMPs) were designed and fabricated for multiplex identification of cell surface markers in HBECs. Cells were probed directly using dark field microscopy integrated with a spectral imager for simultaneous detection of up to three surface markers. The immunophenotype composition of these cell lines indicative of their metastasis potential was assessed using the GNrMPs. The technique has the potential to become an important tool for diagnosis and prognosis of breast and other cancers.

Breast cancer has the highest incidence among women in the western world, affecting up to 10% of women, and therefore is among today's most pressing health concerns.[1] Despite improvements in diagnosis and treatment, the effect on mortality has been modest. Breast cancers metastasize to several organs (17 at least), with lungs, pleura, liver, and bone being major target organs.[2] Metastasis is a complex process involving invasion, intravasation, survival in circulation, arrest in new organ, extravasation, local migration, initiation, and sustained growth at sites of metastasis.[3] Among these steps, invasion, intravasation, survival of cells after extravasation, and growth at sites of metastasis are inefficient processes. Recent studies have shown that tumors are organized in a hierarchy of heterogeneous cell populations with different biological properties and that only a small proportion of tumor cells called the cancer stem cells (CSC) have the capacity to initiate and maintain a malignant tumor.[4] Immunophenotypic categorization of CSCs from blood, brain, and breast,[5−8] usually accomplished by flow cytometry, provides a classification based on the expressed cell surface markers. Such cells are shown to be responsible for tumor formation and endowed with stem/progenitor cell properties.

Recent studies of breast cancer have identified a subpopulation (CD44+/CD24−) of breast cancer cells that demonstrated CSC properties.[8] A direct relationship between progenitor states and invasive capacity of cancer cells (invasion being the first step in the metastasis cascade) was also established via flow cytometry analysis of various breast cancer cell lines for CD44 and CD24 phenotype and subsequent analysis of CD44+/CD24− (progenitors) and CD44−/CD24+ (nonprogenitors) cells for invasion and metastasis using matrigel and xenograft models.[9] It has been reported that five among 13 breast cancer cell lines (MDA-MB-231, MDA-MB-436, Hs578T, SUM1315, and HBL-100) contained a higher percentage (>30%) of CD44+/CD24− cells.[9] Cell lines with high CD44+/CD24− cell numbers express basal/mesenchymal or myoepithelial but not luminal markers. Expression levels of proinvasive genes (IL-1α, IL-6, IL-8, and urokinase plasminogen activator (UPA)) were higher in cell lines with a significant CD44+/CD24− population than in other cell lines. Among the cell lines with CD44+/CD24− subpopulation, MDA-MB-231 has the unique property of expressing a broad range of genes that favor bone and lung metastasis. It has been proposed that breast cancer cells with CD44+/CD24− subpopulation express higher levels of pro-invasive genes and possess highly invasive properties.[9] A recent report by Polyak and co-workers[10] confirmed that CD44+ cell-specific genes included many known stem cell markers and correlated with decreased patient survival. The TGF-β pathway was specifically active in CD44+ cancer cells, where its inhibition induced a more epithelial phenotype. Hence, identification of cells of CD44+/CD24− immunophenotype within a population of tumor cells may have great value in terms of predicting the invasiveness and metastasis potential of the tumor.

* Corresponding author. E-mail: josephi@purdue.edu. Telephone: 765-494-0388. Fax: 765-496-1115.

[†] Department of Agricultural and Biological Engineering, Purdue University.

[‡] Bindley Biosciences Center, Purdue University.

[§] Department of Surgery, Indiana University School of Medicine.

[||] Walther Oncology Center, Indiana University School of Medicine.

[⊥] Department Biochemistry and Molecular Biology, Indiana University School of Medicine.

[#] Walther Cancer Institute.

10.1021/nl070894m CCC: $37.00
Published on Web 06/29/2007

At present, immunophenotypic classification of voluminous cell numbers is accomplished by flow cytometry, which is a fluorescence-based technique where cell surface markers are identified by fluorescence-tagged antibodies.[9] However, due to the broad band, spectral overlap, and the narrow range of the wavelength of visible light (~300−700 nm), fluorescence-based detection can only accommodate limited multiplexing capacity; the upper limit of fluorescence-based multiplexing is ~7 and requires statistical/graphical procedures and deconvolution. Alternatives to small-molecule fluorophores such as quantum dots are narrow-banded and are currently widely used and studied for multiplexing detection applications due to their unique size-dependent fluorescence properties.[11−12] But potential human toxicity and cytotoxicity of the semiconductor material are two major impediments for its implementation, in vitro and in vivo.[13]

Among the nonfluorescence-based alternatives, nanostructures that exhibit plasmonic resonance could serve as potential multiplexers. The tunability of gold nanorod-based molecular probes with noncytotoxic[14] functionalization strategies presents an attractive opportunity. Several studies have reported on the general use of gold nanoparticles and nanostructures as contrast agents for biomedical imaging using confocal scanning optical microscopy,[15] multiphoton plasmon resonance microscopy,[16] optical coherence microscopy,[17] and third harmonic microscopy.[18] Gold nanostructures have several advantages in cellular imaging compared to other agents. They scatter light intensely and are much brighter than chemical fluorophores. They do not photobleach and can be easily detected in as low as 10^{-16} M concentration.[19] More specifically, gold nanorods possess the ability to resonantly scatter visible and near-infrared light upon excitation of their surface plasmon oscillation to transmit an optical signal in the range between 600 and 2000 nm, providing excellent multiplexing capacity (30 probes can be accommodated within this range, with a 50 nm separation in absorbance bands for easy distinction). The scattering light intensity is extremely sensitive to the shape and size of the nanorod as well as the dielectric environment surrounding these nanostructures.[20] Using gold nanorod-based molecular probes, multiple cell surface markers can be interrogated simultaneously, and a simple cell-identity profiling scheme could be developed to profile different immunophenotype of cells.

El-Sayed and co-workers described a detection scheme in which spherical gold nanoparticles were conjugated to anti-EFGR antibodies and incubated with noncancerous and cancerous cells. Binding of gold nanoparticles to the cell surface epidermal growth factor receptor (EGFR) by the anti-EGFR gold nanoparticles was visualized and characterized by dark field microscopy and microspectroscopy. Different binding patterns were observed corresponding to the cancerous and noncancerous cells that can be used as a basis for diagnosis. However, in their approach, only one single cell surface maker (EGFR) could be interrogated due to the limitation posed by the fixed optical property of spherical gold nanoparticles, which is not sufficient for accurate cell identity profiling.[13]

In this letter, we report a procedure to fabricate gold nanorod molecular probes (GNrMP) and deploy these structures for multiplex detection using an optical microscope fitted with a dark field accessory and a prism and reflector imaging spectral system (PARISS). Multiplexing detection of cell surface markers (CD24, CD44, CXCR4 or CD24, CD44, and CD49f) that are of critical importance in metastasis of breast cancer is demonstrated by using their tunable surface plasmon resonance (SPR) characteristics to monitor multiple (up to three) cell surface markers simultaneously for better identity profiling of the immunophenotype of the cancer cells. We also introduce the concept of using an internal reference biomarker that is ubiquitously expressed in all cells for evaluating the relative expression levels of important cell surface markers. In addition, the nonphotobleaching nature of GNrMPs has potential for practical protocol development to allow rapid interrogation of living cells for identity profiling under physiological conditions. The proposed methodology was demonstrated to profile three human breast epithelial cell lines with different malignancy and metastasis status (MCF10A, MDA-MB-436, and MDA-MB-231), and the presence of subpopulations of cells with different immunophenotypes was determined in all cell lines. Dramatic differences in the immunophenotypic composition of the cell lines were observed across all cell lines that can be correlated to invasiveness and metastasis potential.

Gold nanorods with different aspect ratios were prepared by a wet-chemistry, seed-mediated growth method,[20] Three types of gold nanorods with aspect ratios of 1.5, 2.8, and 4.5, respectively, were used for the synthesis of GNrMPs. The seed-mediated growth procedure produced gold nanorods with an initial CTAB coating. CTAB is known to be cytotoxic[21] and is not ideal for in vivo diagnosis. A functionalization strategy to replace CTAB needs to be developed. Although the high binding affinity of alkanethiols to gold has been widely utilized to chemically modify gold nanoparticle surface for biological functionalization;[22−24] it cannot be directly applied to CTAB-capped gold nanorods because the tightly packed CTABs to the side faces of the gold nanorods block the access of alkanethiol molecules to the gold surface. Spontaneous reaction of alkanethiol molecules with gold under ambient temperature occurs only at the end faces of the gold nanorods and results in a partially activated gold nanorods.[22−24] In partially activated gold nanorods, the remaining CTAB, which is positively charged at physiological pH and attracts negatively charged proteins, can cause severe nonspecific binding problems. To overcome this problem, the CTAB cap has to be replaced completely. In this work, the CTAB caps were removed to expose the gold surface to the alkanethiol to initiate a reaction, while at the same time, a mechanism needs to be created to prevent the gold nanorods from aggregation. A procedure was developed in our lab to remove CTAB by elevating the temperature of the solution, and the gold nanorods were kept from aggregation by sonication. 11-Mercaptoundecanoic acid (MUDA) was used as the alkanethiol to react with the gold nanorods to produce a fully activated surface for biofunc-

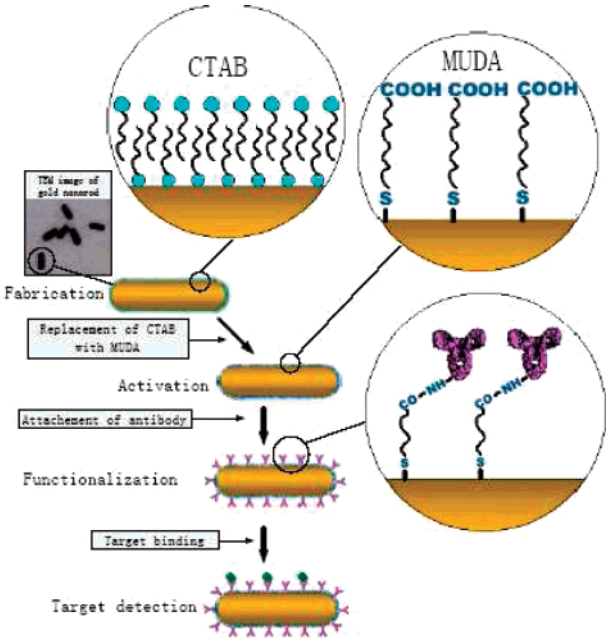

Figure 1. Illustration of the fabrication of gold nanorod molecular probes (GNrMPs). (a) Synthesis of gold nanorods, (b) Activation step to replace the CTAB coating with MUDA, (c) Functionalization and attachment of antibodies to the MUDA anchor, and (d) Target detection, depicting the binding of GNrMPs to their molecular targets.

tionalization. Briefly, the nanorods were suspended in water at 20 nM, to 5 mL of this solution, 1 mL of 20 mM MUDA in ethanol was added, and the solution was kept at 60 °C under constant sonication for 30 min, and then the temperature was decreased to 30 °C, and the solution was kept under constant sonication for 3 h. The solution was then subjected to chloroform extraction for three rounds and the gold nanorods were collected by centrifugation and resuspended in PBS buffer (pH 7.4, Sigma). After activation, the gold nanorods were further functionalized with antibodies against CD24, CD44, CD49f (Pierce Biotechnology, Inc., Rockford, IL), and CXCR4 (R&D Systems, Minneapolis, MN), following the procedure developed in our lab.[20] Briefly, 2.5 mL of activated nanorods (20 nM) was treated with a mixture of 1-ethyl-3-[3-dimethylaminopropyl]carbodiimide hydrochloride (EDC) (0.4 M) and *N*-hydroxysuccinimide (NHS) (0.1 M) then incubated with antibody solution at 0.1 μM at 4 °C under sonication for 30 min. The unbound antibodies were removed by centrifugation, and the remaining free binding sites on the nanorod surface were blocked by treating with 0.1 M ethanolamine solution. The functionalized gold nanorod molecular probes (GNrMPs) were redispersed in PBS buffer at 10 nM and stored at 4 °C. The GNrMPs remained stable for up to 100 days without significant aggregation; the wavelength of the plasmon bands experienced no change within this time period. The intensity of the plasmon bands experienced small drop after 30 days due to minor aggregation, but the change of plasmon band intensity was less than 5% after even 100 days. The whole functionalization process is illustrated in Figure 1. Other functionalization strategies for gold nanorods were also

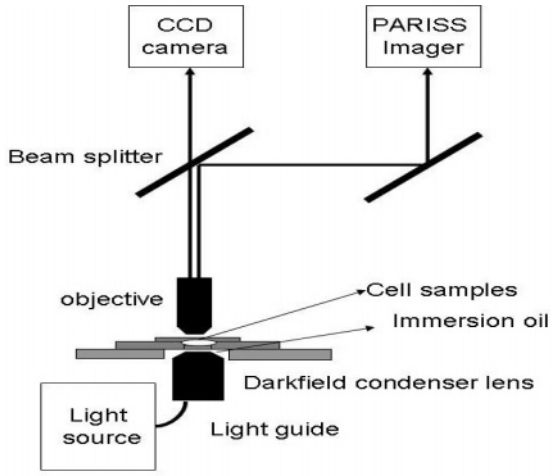

Figure 2. Schematic of the GNrMP detection workstation.

reported, i.e., replacing CTAB by lecithin[25] and thiolated-PEG,[21] our procedure is equally effective due to its ease of implementation and its flexibility to accommodate a variety of biological functional agents, i.e., antibodies, DNAs.

Nonmalignant human breast epithelial cell (HBEC) line MCF10A and two malignant HBEC cell lines (MDA-MB-436 and MDA-MB-231) were cultured on 18 mm diameter glass cover slips in a six-well tissue culture plate. MCF-10A cells were grown in DMEM/F12 media containing 5% horse serum and the following supplements: 10 μg/mL of insulin, 20 ng/mL of epidermal growth factor, 100 ng/mL of cholera euterotoxin, 0.5 μg/mL of hydrocortisone, and 2 mmol/l of L-glutamine. MDA-MB-436 and MDA-MB-231 cells were cultured in DMEM with 10% FCS. The cell cultures were incubated at 37 °C under 5% CO_2. Once the cells reached confluence (48−72 h), 0.5 mL of 10 nM gold nanorod molecular probes (a mixture of all three types) were added to the media and incubated for 30 min at 4 °C to allow binding to the respective cell surface markers. The cells on the cover slips were then rinsed with PBS buffer and sealed with a microscope glass slide with pre-etched chambers containing 100 μL of fresh medium to keep the cells moisturized and in their physiological state. Cells can live up to 1 h under this condition.

Dark field images of the cells were obtained using an Olympus BX40 microscope equipped with a CytoViva dark field module (Aetos Technologies, Inc., Auburn, AL) for dark field imaging where scattering GNrMPs appear as bright particles against a dark background. Imaging was accomplished through collection of the scattered light using a 40× objective. The collected scattered light was further spectrally resolved in a PARISS spectroimager (LightForm, Inc., Hillsborough, NJ) at a spectral resolution ~2 nm and detected with a CCD camera, and the absorption/scattering plasmon spectra of the gold nanorod molecular probes attached to the cell surfaces were obtained as illustrated by the schematic in Figure 2. This setup potentially allows samples to be scanned at a maximum speed of 60 mm/s, which is about 0.5 ms/cell.

The attachment of the GNrMPs to the cell surface markers was confirmed through back-scattering field emission scan-

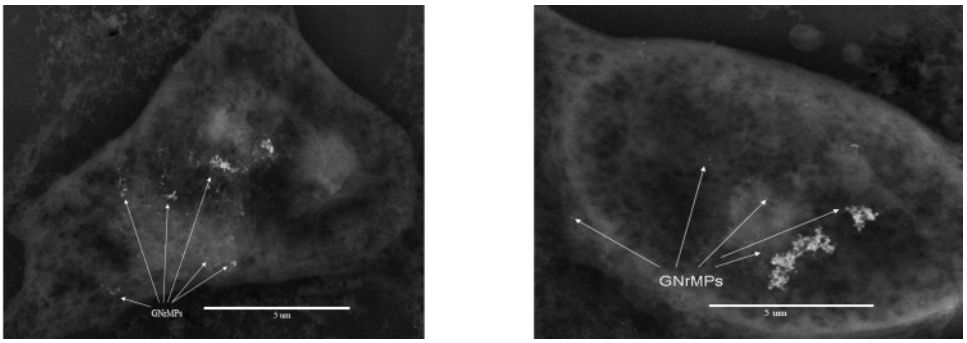

Figure 3. Back-scattering SEM images of MBA MD231 cells confirming the attachment of GNrMPs (CD44 and CD49f) to cell surface marker targets on single cells; GNrMPs appear as individual probes as well as clusters bound to cell surfaces.

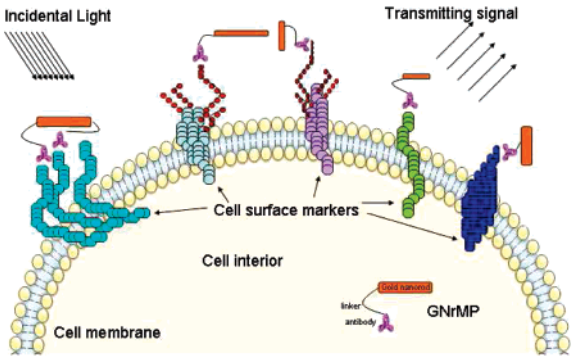

Figure 4. Cell identity profiling for multiplex target detection using GNrMPs.

ning electron microscopy (FEI NOVA nanoSEM field emission SEM, FEI Co., Hillsboro, OR), where CD44/CD49f GNrMPs binding to MDA −MB-231 cells were visualized (Figure 3). Cells were reacted with GNrMPs for 30 min and then washed vigorously using 0.1 M K−Na_2−phosphate buffer (pH 7.4) to remove unbound GNrMPs. The GNrMPs appeared as individual probes binding to cell surface markers. Some of the GNrMPs appeared as larger clusters on the cell surfaces. The direct observation of GNrMPs bound to the cell surface validates the GNrMP scheme. The mechanism of GNrMP-based cell identity profiling is illustrated in Figure 4. GNrMPs designed for different cell surface markers binds to their targets on the cell surface to transmit optical signals that are detected using the PARISS imager. A surface marker that is ubiquitously expressed across all the cell types at RNA level (CXCR4) was used as an internal reference. Among the 13 breast epithelial cell lines investigated by Nakshatri and co-workers, the expression of CXCR4 was found to be the highest at RNA level as measured by Northern blotting in TMD 231 cells, while the cell lines investigated in this study show similar expression level.[9] Hence CXCR4 can be used as an internal reference to evaluate the relative expression levels of other markers (CD24, CD44, and CD49f). The sensitivity of flow cytometry only allows the detection of the cell surface expression of CXCR4 protein in the most highly expressed cells (TMD-231 cells), where as the GNrMP assay yields detectable CXCR4 signals in all the cell lines not possible otherwise.[9] These results suggest increased sensitivity of the GNrMP assay over flow cytometry in detecting cell surface molecules expressed at low levels. Signals from other surface markers (CD24, CD44, CD49f) can be semiquantitatively evaluated based on their relative intensity to the reference, therefore, the expression levels of these markers, which are proportional to the signal intensity of their respective GNrMPs, can be estimated.

Parts a−c of Figure 5 show the dark field image of MCF10A, MDA-MB-436, and MDA-MB-231 cells with no GNrMPs attachment, respectively. Because light is scattered differently by the nucleus and cytoplasm, a good contrast was observed. The morphological characteristics of the three cell lines are quite similar and cannot be used as a criterion for differentiation among the cell lines, especially for the two malignant cell lines (MDA-MB-436 and MDA-MB-231). When the signals were analyzed by the PARISS imager, the characteristic white-light spectrum of the mercury lamp is obtained, as shown in Figure 5d. The scattering and absorption of cells did not alter the spectral characteristics of the transmitted light significantly.

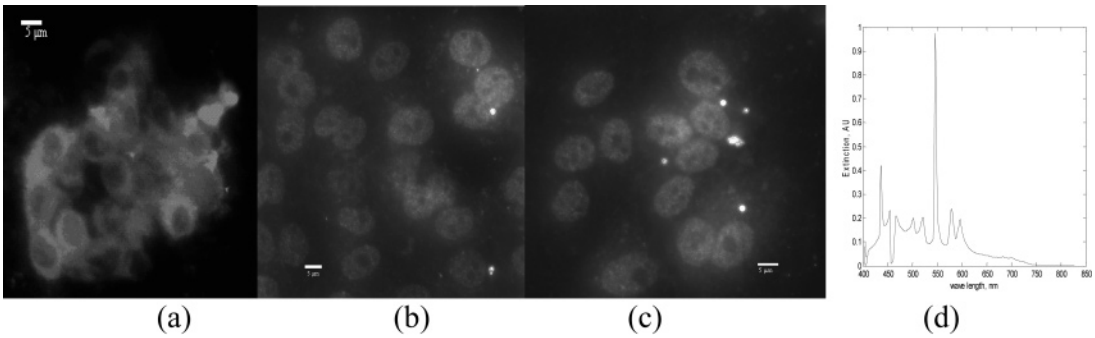

Figure 5. Dark field images of three HBEC lines (a) MCF10A, (b) MDA-MB-436, (c) MDA-MB-231, (d) mean spectrum measured.

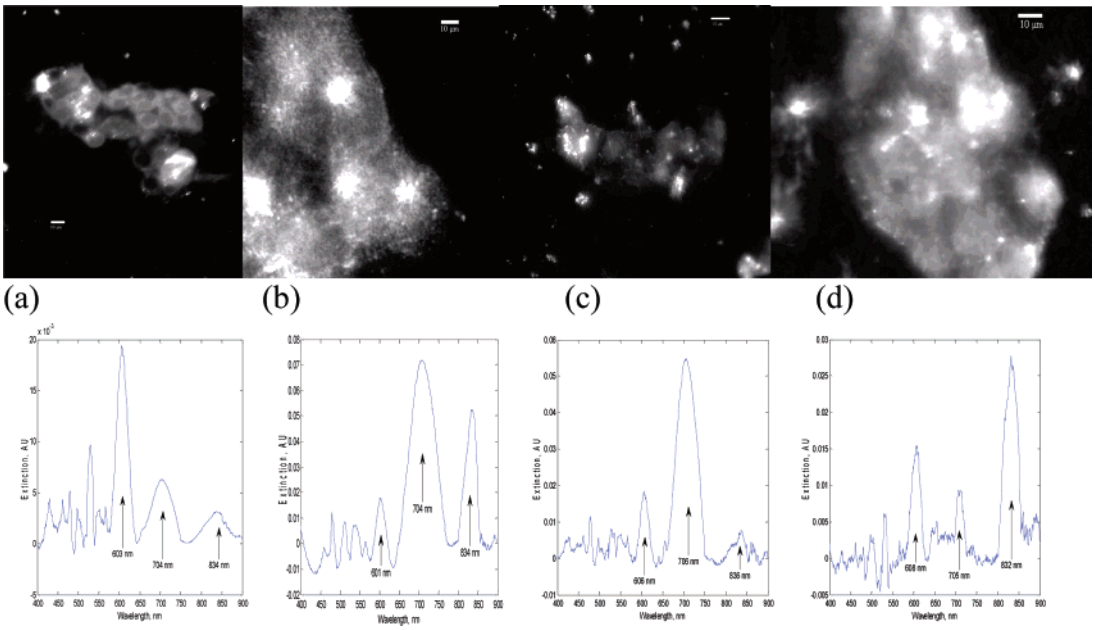

Figure 6. Darkfield images and plasmon spectra of cells displaying different immunophenotypes depicted by the recognition of GNrMPs of three different aspect ratios (1.5, 2.8, and 4.5) by the respective cell surface markers (a) CD24−/CD44− (GNrMP 598:CXCR4; GNrMP690: CD24; GNrMP829:CD44), (b) CD24+/CD44+, (c) CD24+/CD44−, (d) CD24−/CD44+.

Table 1. Immunophenotype Composition of Cell Population of Three HBE Cell Lines

	CD24+/CD44+		CD24−/CD44−		CD24−/CD44+		CD24+/CD44−	
	GNrMP	cytometry	GNrMP	cytometry	GNrMP	cytometry	GNrMP	cytometry
MCF10A, %	6.6	5	62.7	58	14.3	17	16.97	20
MDA MB 436, %	19.8	22	8.1	7	72.1	71	0	0
MDA MB 231, %	3.5	2	12.1	13	84.4	85	0	0

When GNrMPs were applied to the cell samples with intended biomarker targets, dramatically different characteristics were observed depicting the binding of probes to the cell surface marker targets. Parts a−d of Figure 6 show the dark field images of MCF10A cells of different immunophenotypes with the attached GNrMPs and their respective spectra measured by the PARISS spectral imager. In Figure 6a, the contrast between cell nucleus and cytoplasm can still be observed by visual inspection, while stronger scattering of light from a few GNrMPs is also clearly seen. The observed spectrum experienced major changes, and the three bands corresponding to the three GNrMPs indicative of the markers could be identified within the spectrum. CXCR4 band is the most intense; CD24 and CD44 bands are both weaker, suggesting a lower expression level for these two markers compared to CXCR4. Another possibility of the origin of the CD24 and CD44 signals could be due to the nonspecific binding of the respective GNrMPs to other cell surface proteins, as suggested by El-Sayed and co-workers.[13] Under both circumstances, because we know that CXCR4 itself is only expressed at a low to moderate level in HBEC cells,[26] this observation indicates that cells shown in Figure 6a displayed the immunophenotype, CD44−/CD24−. Visual inspection of Figure 6b did not reveal any detailed subcellular structures because the image was dominated by strong scattering light from GNrMPs, indicating the presence of relatively large numbers of GNrMPs on the cell surfaces. The spectral inspection confirms strong signals originating from CD44 and CD24 tethered GNrMPs, compared to the moderately expressed reference of CXCR4, suggesting an immunophenotype of CD44+/CD24+. Compared to Figure 6a, it is clear that the binding of GNrMPs to the cell surface cannot be explained by nonspecific interaction between the GNrMPs and the cells, which further confirmed the immunophenotype as CD44+/CD44+ for these cells. In parts c and d of Figure 6c, immunophenotypes of CD44−/CD24+ and CD44+/CD24− were observed, indicative of the higher expression levels of CD24 and CD44 cell surface markers, respectively.

Another important observation is that all GNrMP signals showed a certain degree of red-shift in the longitudinal plasmon bands upon binding to cell surfaces. The scale of the red-shift varies from 3 to 16 nm for different GNrMPs and different cell immunophenotypes. These shifts were caused by changes in the dielectric environments of the GNrMPs upon binding to cell surface markers, the scale of the shift can be potentially used to quantitatively evaluate the binding affinity of GNrMPs to their targets in a multiplex format.

These observations show that, in MCF10A cells, four immunophenotypes of CD44+/CD24+, CD44−/CD24−, CD44−/CD24+, and CD44+/CD24− all are present; by counting the numbers of each immunophenotype in a cell population, the immunophenotype composition of MCF10A

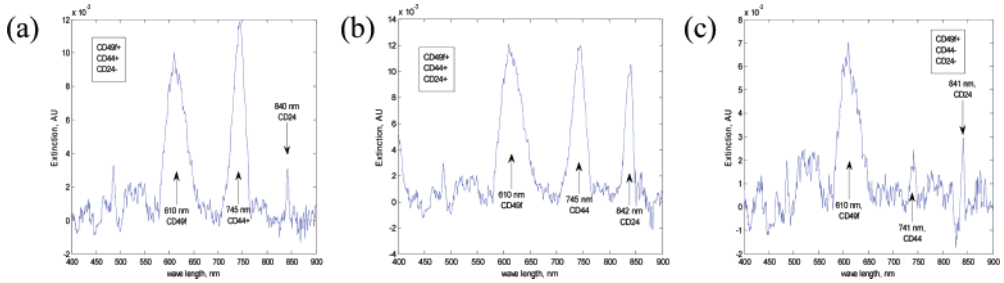

Figure 7. GNrMP plasmon spectra (aspect ratios 1.5, 2.9, 4.5) of MBA MD231 cells with immunophenotypes of (a) CD49f^{h}/CD44+/CD24−, (b) CD49f^{h}/CD44+/CD24+, (c) CD49f^{m}/CD44−/CD24−.

cells as determined is listed in Table 1. In MCF10A cells, the most dominant immunophenotype CD44−/CD24− constitutes 62.7% of the cell population; the highly invasive immunophenotype CD44+/CD24− constitutes ∼14.3% of the cell population, suggesting that MCF10A cell line may not be a highly invasive cell line, consistent with the matrigel and nude mice study reported by Sheridan et al.[9]

When MDA-MB-436 and MDA-MB-231 cells were investigated, a different pattern was observed. As listed in Table 1, in these two cell lines, CD44+/CD24− cells are the most dominant, constituting 84.4% and 72.1% of the cell population, respectively, while the CD44−/CD24+ was not observed at all. These observations strongly suggest that both MDA-MB-436 and MDA-MB-231 cells are highly invasive, with high metastatic potential consistent with the previous reports.[9]

The immunophenotype composition of the cell population acquired by the GNrMP assay as validated by flow cytometry analysis is presented in Table 1. The GNrMP results are in good agreement with flow cytometry results, suggesting that the GNrMP assay developed is an excellent method for cell identity profiling.

In addition to CD24 and CD44, CD49f is another cell surface marker found to be associated with the stemness of breast epithelial cells.[27,28] An immunophenotype of CD49f^{h}/CD24^{+} was reported to indicate normal mouse mammary stem cells.[27,28] However, the correlation between CD49f and human breast CSC is not clear. In this study, GNrMPs with anti-CD49f markers were used to investigate the expression of CD49f in CD44+ and CD44− cells. In MDA-MB-231 cells, as shown in Table 1, CD44+ immunophenotypes constitute 88% of the cell population (3.5% CD24+; 84.4% CD24−). In the CD44+ immunophenotype, CD49f was observed in both CD24+ and CD24− cells, at a relatively high expression level compared to CD44, as shown in parts a and b of Figure 7; while in CD44− immunophenotype, the expression level of CD49f seems to be lower than in CD44+ cells (Figure 7c). These observations suggest that there might be a correlation between high expression levels of CD49f and CD44.

In summary, in this letter, we have reported a novel, nontoxic gold nanorod molecular probe-based multiplexing scheme for identity profiling of breast tumor cells to identify highly invasive CSCs. In the current scheme, three CSC-associated surface markers (CD44, CD24, and CD49f) were monitored simultaneously. Because of the high multiplexing capacity of gold nanorods, the multiplexing capability of the GNrMP assay could possibly be expanded to 15 or greater. The GNrMP scheme can potentially become a powerful tool for single cell identity profiling to examine the evolution or distribution of surface markers as well as for the classification of cells that can eventually lead to better and more accurate diagnosis and prognosis of breast as well as other cancers.

Acknowledgment. We thank Prof. Paul Robinson, Dr. Bartek Rajwa, and Mr. Silas Leaveslay at the Bindley Bioscience Center of Purdue University for use of their spectral imager and microscopic facilities. Partial funding from the Oncological Science Center and IUPUI Walter center grant is acknowledged. This work is also supported partially by Susan G. Komen Foundation grant BCTR0601111 (to H.N.).

References

(1) Greenlee, R. T.; Murray, T.; Bolden, S.; Wingo, P. A. *Ca Cancer J. Clin.* **2000**, *50*, 7−33.
(2) Weigelt, B.; Peterse, J. L.; Vant Veer, L. J. *Nat. Rev. Cancer* **2005**, *5*, 591−602.
(3) Chambers, A. F.; Matrisian, L. M. *J. Natl. Cancer Inst.* **1997**, *89*, 1260−70
(4) Ponti, D.; Costa, A.; Zaffaroni, N.; Pratesi, G.; Petrangolini, G.; Coradini, D.; Pilotti, S.; Pierotti, M.; Daidone, M. *Cancer Res.* **2005**, *65*, 5506−5511.
(5) Bonnet, D.; Dick, J. E. *Nat. Med.* **1997**, *3*, 730−737.
(6) Singh, S. K.; Hawkins, C.; Clarke, I. D.; Squire, J. A.; Bayani, J.; Hide, T.; Henkelman, R. M.; Cusimano, M. D.; Dirks, P. B. *Nature* **2004**, *432*, 396−401.
(7) Singh, S. K.; Clarke, I. D.; Terasaki, M.; Bonn, V. E.; Hawkins, C.; Squire, J.; Dirks, P. B. *Cancer Res.* **2003**, *63*, 5821−8.
(8) Al-Hajj, M.; Wicha, M. S.; Benito-Hernandez, A.; Morrison, S. J.; Clarke, M. F. *Proc. Natl. Acad. Sci. U.S.A.* **2003**, *100*, 3983−3988.
(9) Sheridan, C.; Kishimoto, H.; Fuchs, R.; Mehrotra, S.; Bhat-Nakshatri, P.; Turner, C. H.; Goulet, R., Jr.; Badve, S.; Nakshatri, H. *Breast Cancer Res.* **2006**, *8*, R59−72.
(10) Shipitsin, M.; Campbell, L. L.; Argani, P.; Weremowicz, S.; Bloushtain-Qimron, N.; Yao, J.; Nikolskaya, T.; Serebryiskaya, T.; Beroukhim, R.; Hu, M.; Halushka, M. K.; Sukumar, S.; Parker, L. M.; Anderson, K. S.; Harris, L. N.; Garber, J. E.; Richardson, A. L.; Schnitt, S. J.; Nikolsky, Y.; Gelman, R. S.; Polyak, K. *Cancer Cell* **2007**, *11*, 259−273.
(11) Bruchez, M., Jr.; Moronne, M.; Gin, P.; Weiss, S.; Alivisatos, A. P. *Science* **1998**, *281*, 2013−2015.
(12) Chan, W. C. W.; Nie, S. *Science* **1998**, *281*, 2016−2018.
(13) El-Sayed, I. H.; Huang, X.; El-Sayed, M. A. *Nano Lett.* **2005**, *5*, 829−834.
(14) West, J. L.; Halas, N. J. *Curr. Opin. Biotechnol.* **2002**, *11*, 215−217.
(15) Sokolov, K.; Follen, M.; Aaron, J.; Pavlova, I.; Malpica, A.; Lotan, R.; Richartz-Kortum, R. *Cancer Res.* **2003**, *63*, 1999−2004.

(16) Yelin, D.; Oron, D.; Thiberge, S.; Moses, E.; Silberberg, Y. *Opt. Express* **2003**, *11*, 1385−1391.
(17) Raub, C. B.; Orwin, E. J.; Haskell, R. *J. Biomech. Eng.* **2003**, *125*, 1−6.
(18) Yelin, D.; Oron, D.; Korkotian, E.; Segal, M.; Silberberg, Y. *Appl. Phys. B* **2002**, *74* (Suppl.), S97−S101.
(19) Yguerabide, J.; Yguerabide, E. E. *Anal. Biochem.* **1998**, *262*, 137−156.
(20) Yu, C.; Irudayaraj, J. *Anal. Chem.* **2007**, *79*, 572−579.
(21) Pierrat, S.; Zins, I.; Breivogel, A.; Sonnichsen, C. *Nano Lett.* **2007**, *7*, 259−263.
(22) Chang, J.; Wu, H.; Chen, H.; Ling, Y.; Tan, W. *Chem. Commun.* **2005**, 1092−1094.
(23) Caswell, K. K.; Wilson, J. N.; Bunz, U. H. F.; Murphy, C. J. *J. Am. Chem. Soc.* **2003**, *125*, 13914−13915.
(24) Thomas, K. G.; Barazzouk, S.; Ipe, B. I.; Shibu, J. S. T.; Kamat, P. V. *J. Phys. Chem. B* **2004**, *108*, 13066−13068.
(25) Takahashi, H.; Niidome, Y.; Niidone, T.; Kaneko, K.; Kawasaki, H.; Yamada, S. *Langmuir* **2006**, *22*, 2.
(26) Liang, Z.; Yoon, Y.; Votaw, J.; Goodman, M. M.; Willams, L.; Shim, H. *Cancer Res.* **2005**, *65*, 967−971.
(27) Wang, R. *Int. J. Biol. Sci.* **2006**, *2*, 186−187.
(28) Stingl, J.; Eirew, P.; Ricketson, I.; Shackleton, M.; Vaillant, F.; Choi, D.; Li, H. I.; Eaves, C. J. *Nature* **2006**, *439*, 993−997.

NL070894M